Regional deficits in endogenous regeneration of mouse olfactory sensory neuron axons

Tenzin Kunkhyen[1], Kendall A. Curtis[1], Thomas P. Deakin[1], Jane S. Huang[1], Jordan D. Gregory[1,2] & Claire E.J. Cheetham[1]

[1] Department of Neurobiology, University of Pittsburgh

[2] Center for Neuroscience at the University of Pittsburgh

Author Contributions

Conceptualization: T.K., K.A.C. and C.E.J.C; Methodology: T.K & C.E.J.C; Software: J.S.H., Formal Analysis: K.A.C., T.P.D., J.D.G and C.E.J.C; Investigation: T.K., K.A.C., T.P.D. and C.E.J.C; Data Curation: C.E.J.C; Writing – Original Draft: C.E.J.C; Writing – Review & Editing: T.K., J.S.H, J.D.G and C.E.J.C; Visualization: C.E.J.C; Supervision: T.K. and C.E.J.C; Project Administration: C.E.J.C; Funding Acquisition: C.E.J.C.

Abstract

Postnatal neurogenesis occurs in only a few regions of the mammalian nervous system. Hence, neurons that are lost due to neurodegenerative disease, stroke, traumatic brain injury or peripheral neuropathy cannot be replaced. Transplantation of stem cell-derived neurons provides a potential replacement strategy, but how these neurons can be encouraged to functionally integrate into circuits remains a significant challenge. In the mammalian olfactory epithelium (OE), olfactory sensory neurons (OSNs) continue to be generated throughout life from basal stem cells and can be repopulated even after complete ablation. However, the specialized population of navigator OSNs that ensures accurate odorant receptor-specific targeting of OSN axons to glomeruli in the olfactory bulb (OB) is only present perinatally. Despite this, some studies have reported complete regeneration of specific glomeruli, while others have found various degrees of recovery, following OSN cell death. Variability in the extent of both initial OSN ablation and subsequent repopulation of the OE, and the focus on anatomical recovery, leave the extent to which newly generated OSNs can reinnervate the OB unclear. Here, we employed the olfactotoxic drug methimazole to selectively ablate OSNs without damaging the basal stem cells that generate them, enabling us to assess the extent of functional recovery of OSN input to the OB in the context of complete OSN repopulation. We found profound deficits in the recovery of odor-evoked responses in OSN axons in the glomerular layer of the dorsal OB five weeks after OSN ablation, a time point at which OSNs are known to have repopulated the OE. Histological analysis of mature OSN axons in the OB at 10 and 20 weeks post-methimazole showed a persistent region-specific deficit in OSN axon reinnervation of the dorsal OB, with the dorsomedial region being particularly adversely affected. In contrast, reinnervation of the ventral, lateral and medial regions of the OB was almost complete by 10 weeks post-MMZ. Hence, we have identified a region-specific deficit in OSN reinnervation of the mouse OB, which sets the stage to identify the mechanisms that mediate successful vs. unsuccessful axonal regeneration in an endogenous population of stem cell-derived neurons.

Introduction

Most mammalian neuronal types are generated only during embryonic and early postnatal development, meaning that in the adult nervous system, lost or damaged neurons cannot be replaced. In contrast, olfactory sensory neurons (OSNs) continue to be generated throughout life from basal stem cells in the olfactory epithelium (OE) of the nose of all terrestrial mammals[1–3]. OSNs therefore provide an opportunity to understand how an endogenous population of stem cell-derived neurons wires into highly organized neural circuits throughout life. Determining how OSNs achieve this, and particularly the extent to which OSN input to the brain can recover after substantial damage, will define mechanisms that may promote functional integration of transplanted stem cell-derived neurons to replace lost neurons elsewhere in the brain.

OSNs transmit odor input to the olfactory bulb (OB), with the axons of OSNs that express the same olfactory receptor coalescing together to form glomeruli[4]. Each mature OSN expresses a single olfactory receptor[5–7], which is expressed both on the cilia that protrude from the apical dendritic knob into the mucus layer on the surface of the OE, and on the axon, where it plays an important role in axon guidance[8–11]. The receptor therefore determines both the odor(s) that an OSN can bind and the glomerulus to which it projects its axon. Hence, there is a highly organized odor input map to the brain.

Globose basal cells (GBCs) generate newborn OSNs constitutively throughout life, with each OSN having a half-life of approximately one month[12–15]. In contrast, horizontal basal cells (HBCs) are normally quiescent and generate newborn OSNs only at key developmental time points and to enable repopulation following large-scale OSN cell death[16–18]. OSNs take 7-8 days from terminal cell division to reach maturity, which is defined by the onset of expression of the olfactory marker protein (OMP)[19–22]. During this time, in order to functionally integrate into the olfactory system, each OSN must select a single olfactory receptor, extend a dendrite to the apical surface of the OE, and project an axon to form synaptic connections with OB neuron dendrites in an appropriate glomerulus.

Anatomical recovery of the OSN population in the OE and of axonal projections to the OB has been studied using a variety of methods that induce OSN cell death, yielding

mixed results. Olfactory nerve transection results in degeneration of OSN cell bodies and axons, but lost OSNs are rapidly replaced and reinnervate OB glomeruli with 2-5 weeks[23,24]. Similarly, the effects of treating the OE with Triton X-100 are reversible, with repopulation of the OE with OSNs and reinnervation of OB glomeruli occurring within 6 weeks, albeit with some disorganization of axonal projections[25]. Following inhalation of methyl bromide (MeBr) gas, most areas of the OE recover within six weeks although there is some persistent damage, and there is substantial reinnervation of OB glomeruli within 4-8 weeks, particularly in the anterior OB[26]. In contrast, treatment of the OE with zinc sulfate causes complete loss of the OE, resulting in long-term deficits in OSN repopulation and OB reinnervation even many months later[27]. More recently, systemic administration of methimazole (MMZ) has emerged as a popular model of OSN regeneration, as it avoids the confounds inherent to topical application, leaves the lamina propria intact[28], and spares basal cells such that OSNs can repopulate the OE in 4-12 weeks, depending on MMZ dosage[29–32].

Recovery of the olfactory receptor-specific topography of OSN projections to glomeruli has also received considerable attention. After selective ablation of nearly all OSNs expressing the P2 odorant receptor via a genetic approach, new P2-expressing OSNs accurately reinnervated the original P2 glomeruli in the OB[33]. In contrast, some degree of mis-targeting of OSN axons was seen after large-scale OSN cell death induced by several different methods. Following olfactory nerve transection, P2-expressing OSN axons projected to multiple widely distributed loci in the OB at 10 weeks, and while some further refinement occurred by 18 weeks, there were still more smaller P2 glomeruli than in control mice[34]. Similarly, 18 weeks after systemic dichlobenil treatment, a time point at which a significant number of P2-expressing OSNs have repopulated the OE, P2-expressing axons still terminated in numerous widely dispersed glomeruli[35]. After MeBr inhalation, 2A4(+) OSNs projected to 2-15-fold more glomeruli than in untreated mice, a projection pattern that was maintained up to five months post-treatment[36]. Following MMZ treatment, the accuracy of axonal targeting was better, but deficits remained. At three months post-MMZ, M72-expressing OSN axons largely projected to glomeruli in the expected dorsolateral location, but there were some wandering axons that were not pruned, as well as supernumerary M72 glomeruli[37]. Axonal projections of I7-expressing OSNs to ventral glomeruli largely

recovered by 6 weeks post-MMZ, but formed two glomeruli within a small spatial region, rather than the expected one[37].

There are only three studies that have assessed functional recovery of odor input to the OB. The first study used *in vivo* synapto-pHluorin imaging of odor-evoked responses in the OB to directly assess functional recovery after MeBr treatment[38]. Substantial recovery of odor-evoked responses on the dorsal surface of the OB was seen, including reestablishment of odor-evoked response map topography. However, there was also evidence for atypical convergence of OSN axons, forming smaller glomeruli with less well-defined boundaries, especially when a high dose of MeBr was used[38]. Notably, OSN density did not recover fully after MeBr treatment, which may account for the deficits in OSN reinnervation of the OB[38]. The second study assessed recovery of behavioral performance six weeks after methimazole treatment and found significant recovery for a previously learnt odor discrimination task, but limited recovery of innate aversion to TMT[37]. The final study employed slice electrophysiology to show that functional reconnection of OSN axons with OB neurons occurs rapidly between 13-16 days after MMZ treatment, with presynaptic release probability already high, but some additional maturation occurring over the following week[29].

Therefore, important questions remain about the extent to which OSN axons can accurately reinnervate the OB to provide odor input to OB neurons. In this study, we employed MMZ treatment to address these questions, because it does not damage the lamina propria or basal stem cell population, enabling complete OSN repopulation of the OE. We found profound deficits in OSN reinnervation of the dorsal region of the OB, with the dorsomedial region recovering particularly poorly. Recovery of odor-evoked responses in the dorsal OB was very limited, and OMP immunohistochemistry in fixed tissue confirmed dorsal-specific deficits in reinnervation of dorsal glomeruli that persisted at 20 weeks post-MMZ. In contrast, there were few, if any, differences between medial, lateral and ventral OB glomeruli in MMZ-treated vs. control mice.

Methods

Experimental animals

Animal procedures conformed to National Institutes of Health and ARRIVE guidelines and were approved by the University of Pittsburgh Institutional Animal Care and Use

Committee. Mice were maintained on a 12 h light/dark cycle in individually ventilated cages at 22 °C and 48 % humidity with unrestricted access to food and water unless otherwise stated. Mice were group-housed if same sex littermates were available.

C57BL/6J mice (strain #000664) were purchased from The Jackson Laboratory while other lines were bred in-house. Generation of the OMP-IRES-tTA[39] and tetO-GCaMP6s[40] (Jax #024742) lines has been published. Each experimental group comprised approximately equal numbers of male and female mice. Mice were genotyped by PCR using previously validated primers[40–44]. Experimental mice were C57BL/6J or OMP-GCaMP6s [OMP-IRES-tTA$^{+/-}$;tetO-GCaMP6s$^{+/-}$]. A total of 23 mice were used in this study.

Methimazole ablation of OSNs

Mice received a single intraperitoneal injection of 75 mg/kg methimazole dissolved in sterile saline. For chronic imaging, an equivalent volume of sterile saline was administered to control mice. For immunohistochemistry, age matched (18- or 28-week-old) C57BL/6J mice were purchased as controls and did not receive saline.

Cranial window implantation and headbar attachment

8-10-week-old OMP-GCaMP6s mice were anesthetized with isoflurane (4% for induction, 1.5-2% for maintenance, in 1l/min O_2) and received 5 mg/kg ketoprofen. A 3 mm diameter craniotomy over both OBs was made and a 3 mm diameter glass coverslip was implanted using superglue and dental cement before re-suturing the scalp, as described in detail[45]. Two weeks later, the scalp was removed, and a head bar was attached to enable reproducible repositioning under the 2-photon microscope.

Chronic *in vivo* 2-photon imaging and data analysis

Mice were lightly anesthetized with 5 mg/kg dexmedetomidine and 1% sevoflurane. Chronic *in vivo* 2-photon imaging was performed using a Bergamo II 2-photon microscope (ThorLabs) equipped with a SemiApo 20x/1.0NA water-immersion objective (Olympus) and an Insight X3 IR laser (Newport) mode-locked at 935 nm. Time-lapse images were collected at 15 fps and were 656 μm^2 (pixel size 1.28 μm). Odorant stimulation was performed using a custom-built Arduino-controlled olfactometer. Stimulation and image acquisition timing were controlled and recorded

using a custom-written Python-based user interface, ThorSync and ThorImage 4.0 or 4.1 (ThorLabs). The odorant panel consisted of seven odorants known to activate the dorsal surface of the OB: ethyl butyrate, hexanal, 2-hexanone, propionic acid, isoamyl acetate, methyl salicylate and acetophenone (all 1% v/v dilutions in mineral oil). Saturated vapor from odorant vials, or a blank stimulus consisting of deodorized dehumidified air, were delivered into the anesthetic carrier stream at a constant flow rate of 1 l/min. Odor triggering and delivery were checked before each imaging session. Because we expected no or minimal odorant-evoked responses at early time points post-MMZ, we designed our experiments such that we always imaged a saline-injected mouse on the same day as an MMZ-injected mouse. This ensured that an absence of odorant-evoked responses in an MMZ-injected mouse could be attributed to the MMZ treatment rather than any technical issues.

Image trials were 20 s in duration, consisting of 4s baseline, a 1s stimulus and 15 s post-stimulus. Three trials were delivered for each stimulus, in a randomized order with 90 s between trials. Data was collected for two to three fields of view (FOVs) per mouse. For each FOV, the xyz co-ordinates of the imaged location were recorded, and a widefield camera image of the surface vasculature was captured, to enable the same locations to be re-imaged at subsequent time points. One week later, each mouse was anesthetized and the same FOVs were identified using the XY co-ordinates of the microscope system, the pattern of surface vasculature and the pattern of baseline GCaMP6s fluorescence in glomeruli, when present (note that this latter parameter was less useful in MMZ-treated mice due to gradual degeneration of existing OSN axons). Odor-evoked responses were collected as for the first imaging session. Mice received either MMZ or saline immediately after the second imaging session. Windows were inspected each week for the presence of any bone regrowth that could occlude the imaged FOVs, and imaging was repeated every week for 10 weeks if windows remained clear. Only mice with at least 7 weeks of imaging sessions were included in the analysis. Imaging occurred discontinuously for longer time periods (up to 21 weeks) for some mice in which windows remained clear.

Images were analyzed using two approaches, both in Fiji[46]. In the glomerulus-based approach, individual glomeruli were outlined in the week 1 images. For each stimulus, the three trials were averaged, and a maximum intensity projection (MIP) was

generated. Outlines of all visible glomeruli were drawn for the first stimulus MIP using the polygon tool, superimposed on each subsequent stimulus MIP, and additional visible glomeruli were outlined until all eight MIPs had been completed, to generate the final set of glomeruli for analysis. The unbiased grid-based approach was designed to detect any recovery of odor-evoked responses in MMZ-treated mice, including in locations that did not previously respond and so could be missed using the glomerulus-based approach. A 16-square grid (20.5 μm per square) was overlaid on each image irrespective of glomerular position. Mean fluorescence intensity was then extracted for each glomerulus or grid square for each trial. All images were analyzed using both approaches.

Perfusion, immunohistochemistry, widefield microscopy and image analysis

Perfusion, OB dissection, cryopreservation and sectioning were performed as described[47]. Three coronal OB sections per mouse at 25%, 50% and 75% along the anterior-posterior axis were stained to detect OMP using anti-OMP primary antibody (#544-10001, Wako Chemicals; 1:5000, 96 h at 4 °C) and donkey anti-goat-Alexa Fluor 546 (AF546) secondary antibody (1:500, 1 h at room temperature). Sections were mounted using Vectashield containing DAPI. Tiled images of DAPI and OMP signals throughout entire OB sections were acquired using a Revolve microscope with Echo software (Echo) equipped with a 10x Plan Apo 0.4 NA air objective (Olympus). Bandpass excitation and emission filter wavelengths were (in nm): DAPI (385/30, 450/50) and OMP-AF546 (530/40, 590/50). Images were stitched using Affinity Photo software (Affinity) to generate a complete image of each section.

Image analysis was performed using Fiji (ImageJ)[46]. The glomerular layer (GL) was outlined in the DAPI channel of each section and subdivided into dorsomedial, dorsolateral, medial, ventral and lateral regions. The area and Feret diameter of each GL region was determined. Individual glomeruli were also outlined in the DAPI channel, with outlines verified and edited in the OMP channel. The number of glomeruli in each GL region was counted, using both the DAPI and OMP channels to ensure that all glomeruli were counted. Glomerular linear density was defined as the number of glomeruli within a GL region divided by the Feret diameter of that region. The area and circularity [4π(area/perimeter^2), where a value of 1.0 indicates a perfect circle] of

each glomerulus were also determined. The percentage of the GL occupied by glomeruli was determined for each GL region using the total region area and the summed area of all glomeruli therein. We then calculated the background fluorescence, using 300-pixel diameter circles located in the dorsal, medial, ventral and lateral external plexiform layer. This background fluorescence value was used to threshold the OMP channel to determine the area fraction, i.e. the percentage of each glomerulus filled by OMP+ pixels.

Statistics

Data were analyzed using Prism 10 (GraphPad) with alpha = 0.05. For comparison of glomerulus- and grid-based OMP-GCaMP6s values, data passed the Shapiro–Wilk test for normality and were analyzed using one- or two-way ANOVA. For analysis of OMP-stained OB sections, data passed the Shapiro–Wilk test for normality and were analyzed using two-way ANOVA with Holm-Sidak's multiple comparisons tests between 10-week MMZ vs. control and 20-week MMZ vs. control groups. The details of all statistical tests and their outcomes are provided in the figure legends.

Results

Poor recovery of odorant-evoked responses in dorsal OB glomeruli after MMZ treatment

To determine the timeline and extent of recovery of odor-evoked responses in mature OSN axons in the OB after MMZ treatment, we implanted adult OMP-GCaMP6s mice with OB cranial windows (Fig. 1a), followed by head bars to enable reproducible repositioning under the 2-photon microscope. Three weeks after window implantation, we performed a baseline 2-photon imaging session of responses evoked by a panel of seven odorants known to activate glomeruli on the dorsal surface of the OB. A second baseline imaging session was performed one week later, immediately after which mice were treated with either 75 mg/kg MMZ or saline as a vehicle control. Subsequent imaging sessions were performed weekly for at least five weeks post-treatment (Fig. 1b,c).

Analysis of chronic functional imaging data in the OB has typically involved comparison of odorant response amplitudes within individual glomeruli over time[38,48–50]. However, we reasoned that regeneration of OSN input to the OB might occur

outside the glomerular regions that were defined prior to MMZ treatment based on their baseline GCaMP6s fluorescence and/or responsiveness to one of the tested odorants. Therefore, we developed an unbiased grid-based approach to measure odorant-evoked responses in the same fields of view over time (Fig. 2a). We validated this grid-based approach by comparison to the data from glomerulus-based analysis using data from saline-treated mice. The amplitude of responses varied somewhat over time but was broadly similar across seven weeks of imaging (Fig. 2b), similar to a previous study[38]. The amplitudes of odorant-evoked responses were consistently larger in glomeruli than in grid squares (Fig. 2c), as would be expected given the inclusion of non-odorant-responsive areas within grid squares. However, the ratio of glomerulus to grid responses amplitudes was similar across odorants (Fig. 2d). Therefore, we concluded that the grid-based approach could be used to detect recovery of odorant-evoked responses anywhere in the imaged fields of view in MMZ-treated mice.

We next used our grid-based approach to assess recovery of odorant-evoked responses in MMZ-treated mice. Responses in weeks 1 and 2, prior to MMZ treatment, were similar, with no difference in odorant-evoked response amplitude or the percentage of grid squares that were activated by at least one odorant (Fig. 2e,f). One week after MMZ treatment (imaging week 3), odorant-evoked responses were completely absent (Fig. 2e,f; imaging week 3), confirming that MMZ had resulted in OSN ablation. Odorant-evoked responses remained completely absent at two weeks post-MMZ (imaging week 4), but by three weeks post-MMZ (imaging week 5), small areas of odorant-responsive axons were present in some mice. Surprisingly, neither the amplitude of odorant-evoked responses (Fig. 2e), nor the percentage of grid squares responding to at least one odorant (Fig. 2f) increased further at five weeks post-MMZ (imaging week 7), a time point at which the OE has been repopulated with OSNs[30,32]. Indeed, in a subset of mice in which we performed additional imaging sessions over longer time periods, even up to 17 weeks post-MMZ (imaging week 19), we observed no further recovery of odorant-evoked responses beyond that seen at 3 weeks post-MMZ (imaging week 5; Fig. 2g,h). Overall, we concluded that recovery of odorant-evoked responses in the dorsal OB following MMZ treatment is limited, and indicates a deficit in mature OSN reinnervation of the dorsal OB.

Region-specific deficits in OSN reinnervation 10 and 20 weeks after MMZ treatment

To determine whether the deficits in OSN reinnervation suggested by our *in vivo* calcium imaging data were specific to the dorsal surface of the OB, we employed an immunohistochemical approach that enabled us to analyze entire OB sections. 8-week-old C57BL/6J mice were injected with MMZ and perfused 10 or 20 weeks later, to allow for the possibility that further regeneration might occur over longer time periods than were consistently feasible to assess using our *in vivo* imaging approach. Age-matched control C57BL/6J mice were also perfused, and OB sections from MMZ-treated and control mice were stained for OMP to detect mature OSN axons.

We observed that OMP staining was less extensive on the dorsal surface of the OB of MMZ-treated mice compared to controls, with fewer glomeruli present and some glomeruli lacking innervation by OMP+ OSNs (Fig, 3). It was also apparent that these differences were not uniform throughout the dorsal region of the OB (Fig. 3). Therefore, we subdivided the GL into dorsomedial (DM), dorsolateral (DL), medial, lateral and ventral regions for quantitative analysis (Fig. 4a).

We first determined whether the density of glomeruli within each region of the GL was affected at 10 or 20 weeks post-MMZ treatment. Somewhat surprisingly, glomerular density was similar across much of the GL, although glomerular density was significantly higher in the DL region at both 10 and 20 weeks post-MMZ compared to controls (Fig. 4b). We reasoned that if the area of the GL was also affected by MMZ treatment in certain regions, there could be fewer glomeruli but no change in glomerular density. Therefore, we next determined the percentage of the GL that was occupied by glomeruli for each region. Indeed, we found that the percentage of the GL occupied by glomeruli was significantly lower in both the DL and DM regions at both 10 and 20 weeks post-MMZ, with the magnitude of this reduction being greater in the DM region (DL 10 week -36%; DL 20 week -38%; DM 10 week -75%; DM 20 week: -64%; Fig. 4c). In contrast, there was no difference in the percentage of the GL occupied by glomeruli in the lateral, medial, or ventral regions between MMZ-treated and control mice at either time point (Fig. 4c). Therefore, we concluded that MMZ treatment causes a persistent reduction in the number of glomeruli in the dorsal GL, with this effect being particularly pronounced in the DM region.

We next analyzed the impact of MMZ treatment on the glomeruli themselves. We first determined the impact of MMZ treatment on glomerular size across GL regions. At 10 weeks post-MMZ, glomerular perimeter was significantly smaller in the DL, DM, lateral and medial regions compared to controls, whereas glomerular perimeter was unaffected in the ventral GL (Fig. 4d). By 20 weeks post-MMZ, glomerular perimeter remained significantly smaller in the DL and DM regions, but there was no longer a difference in the lateral or medial regions, with the ventral GL again unaffected (Fig. 4d). We also analyzed the circularity of glomeruli to determine whether the shape of glomeruli that regenerated following MMZ treatment differed from glomeruli in control mice. Glomerular circularity was unaffected by MMZ treatment, except for a subtle but significant decrease in circularity in the DL region at 20 weeks post-MMZ (Fig. 4e). We therefore concluded that MMZ treatment results in smaller glomeruli throughout the dorsal, lateral and medial GL, but this effect is more persistent in the dorsal OB. In contrast, glomerular shape was minimally impacted by MMZ treatment.

The final parameter that we analyzed was the percentage of individual glomeruli that was occupied by OMP+ OSN axons, to provide a measure of glomerular filling by mature OSN axons. We found that in the DM region, the percentage of a glomerulus that was filled by OMP+ axons was strongly and significantly reduced at 10 weeks post-MMZ (mean reduction 43%, $P < 0.001$; Fig. 4f). By 20 weeks, the difference was no longer statistically significant in the DM region, although there was still a trend towards smaller values (mean reduction 17%, $P = 0.084$; Fig. 4f), suggesting some degree of ongoing recovery between 10 and 20 weeks post-MMZ. There was no difference in this parameter for the DL, lateral, medial or ventral regions. Hence, we concluded that there was a selective deficit in reinnervation of DM region glomeruli by mature OSNs following MMZ treatment that gradually recovers over long time periods.

Discussion

Region-specific deficits in OB reinnervation after MMZ treatment

Regional differences in the extent to which newly generated OSN axons can reinnervate the OB have not previously been described. Using multiple different measures to assess the extent of recovery, we found marked deficits in reinnervation of dorsal OB glomeruli by new OSN axons that were particularly pronounced in the dorsomedial region. The most marked regional difference was in the percentage of

glomeruli that was occupied by OMP+ axons, which was dramatically reduced only in the dorsomedial GL 10 weeks post-MMZ. In contrast, two previous studies that used very similar measures of glomerular filling by mature OSN axons found recovery of this parameter within 28 days (after 75 mg/kg MMZ)[30] or 45 days (after 100 mg/kg MMZ)[29]. A key difference is that we analyzed all glomeruli in each coronal section and analyzed the dorsomedial and dorsolateral regions separately, based on initial observations. In contrast, both previous studies[29,30] sampled a much smaller number of glomeruli distributed throughout the GL, so differences in dorsomedial glomeruli could have been missed or masked by averaging. In addition, differences in C57BL/6 mouse sub-strain or other experimental factors that alter the extent of OSN axon reinnervation could contribute to the discrepancy between our data and these previous studies[29,30].

Blanco-Hernández et al. took a different approach to assess recovery of specific glomeruli after treatment with 75 mg/kg MMZ, using tagged OR lines[37]. In line with our findings of extensive reinnervation of ventral and lateral glomeruli, Blanco-Hernández et al. found that projections of I7-expressing OSN axons to glomeruli in the ventrolateral OB recovered within 45 days of MMZ, but axons projected to two adjacent glomeruli, rather than the one glomerulus seen in untreated mice. They also found good recovery of M72-expressing OSN axons to the dorsolateral M72 glomerulus, albeit with many misrouted axons present even 90 days post-MMZ. This finding is not inconsistent with our data: while we found a reduced density of smaller glomeruli, there were many glomeruli present in the DL region at 10-20 weeks post-MMZ. Furthermore, the persistence of misrouted M72-expressing OSN axons supports our finding of deficits in reinnervation of dorsal surface glomeruli after MMZ treatment.

Limited functional recovery of odor-evoked responses on the dorsal OB surface

Chronic imaging to track the extent to which neurogenesis restores odor-evoked responses following OSN cell death is only feasible for the dorsal surface of the OB. We found no recovery of odor-evoked responses in three of the six MMZ-treated mice that we imaged, and only very limited recovery in the other three, even up to 19 weeks after MMZ treatment. Collectively, less than 10% of the originally responding grid squares recovered a response to any odorant in the panel, and mean response

amplitudes were an order of magnitude smaller than in the same fields of view imaged before MMZ treatment.

The only other study to use chronic imaging to assess functional recovery of odor-evoked responses in OSN axons used MeBr inhalation to ablate OSNs[38]. Cheung et al. found that synaptopHluorin response magnitudes recovered to near control levels after 12 weeks, and that functional topography also recovered, with odorants evoking glomerular responses in similar regions to those before treatment. This contrasts with the poor functional recovery that we saw after MMZ treatment. However, Cheung et al. also found that glomeruli were smaller and had less well-defined borders, and that there were areas in which glomeruli were absent in some mice, in good agreement with our data. Why there was good recovery of odor-evoked synaptoHluorin responses yet clear deficits in anatomical reinnervation in Cheung et al. is unclear. One factor that may be important is the variability in response to MeBr exposure across mice; indeed, only six out of ten MeBr-exposed mice were further analyzed in the Cheung et al. study, because the other four showed persistent odor-evoked responses four days after MeBr treatment, indicating a lack of OSN ablation. Another key factor in interpreting data from both MMZ and MeBr studies is recovery of the OE. MeBr can cause persistent loss of globose basal cells in the OE, resulting in areas that are not repopulated with OSNs, in a dose-dependent manner[26,38,51]. Not surprisingly, the extent of OB reinnervation by OSN axons correlates with OSN repopulation in the OE[26]. Hence, the incomplete OSN repopulation that was seen in Cheung et al. may account for deficits in glomerular reinnervation. In contrast, the OE can completely repopulate with OSNs after MMZ treatment, albeit taking longer (90d vs. 28d) when the dose is higher (100 mg/kg vs. 75 mg/kg)[29–31]. Hence, it is likely that the poor functional recovery of odor-evoked responses in the dorsal OB that we observed after MMZ treatment reflects a deficit in axonal reinnervation despite complete OSN repopulation. The mechanisms underlying this region-specific deficit in reinnervation will be important to elucidate in future studies.

Two other studies have provided alternative readouts of functional recovery after MMZ treatment. Browne et al. found rapid reconnection of OSNs with external tufted cells between 13 and 16 days post-MMZ[29]. They recorded from external tufted cells near medial and lateral glomeruli, which explains why they did not see the dorsal-specific

deficits in OSN reinnervation that we observed. Blanco-Hernández et al. observed complete recovery of previously learnt odor discrimination tasks involving M72 and I7 receptor ligands, and partial recovery of innate aversion to TMT[37]. These mixed results likely reflect the anatomical location and extent of reinnervation of the glomeruli responsible for each behavior. Innate responses to TMT are mediated by both dorsal and ventral glomeruli[52,53], so the deficit in OSN reinnervation of the dorsal OB that we observed could underlie the partial recovery of TMT innate aversion seen by Blanco-Hernández. In contrast, Blanco-Hernández demonstrated significant reinnervation of the dorsolateral M72 glomerulus and the ventral I7 glomerulus, supporting the recovery of odor discrimination tasks employing their cognate ligands. It is also likely that behavioral recovery can occur even when glomeruli are only partially reinnervated, based on our previous studies at early time points post-MMZ in which mice could perform odor detection and discrimination tasks using only a small number of new, immature OSNs[47].

Glomerular regeneration in the context of a developmental critical period

Regeneration of OB glomerular maps after OSN cell death requires accurate receptor-specific reinnervation of appropriate glomerular targets. During development, Glomerular maps become immutable after the closure of a perinatal critical period for OSN axon targeting[54,55]. Critical period closure correlates with cell death of a specialized population of navigator OSNs, which help ensure accurate targeting of OSN axons to appropriate glomeruli but are only present perinatally[56]. The absence of navigator OSNs in the adult OE raises the question of how accurate glomerular reinnervation might be achieved. Yet, multiple studies have shown substantial or complete recovery of glomerular targeting after OSN ablation[23,25,29,33,35,37,38,57]. One possible explanation is that degenerating OSN axons provide a pathway for glomerular targeting via homotypic interactions between odorant receptors[26,55,56]. This seems plausible given that degenerating axons are present for at least two weeks after MMZ treatment[29,30], and the first newborn OSNs begin to reinnervate the OB as early as five days post-MMZ[47]. However, it leaves open the question of why there is a selective deficit in reinnervation of dorsal, and particularly dorsomedial, glomeruli after MMZ treatment. Region specific differences in the number of projecting OSN axons, or the rates of OSN axon degeneration vs. arrival of new OSN axons could play a role. In addition, axon guidance mechanisms that specify projections along the dorsal-

ventral axis of the OB could be responsible. Both Slit-Robo and semaphorin-neuropilin expression gradients play important roles in dorsoventral patterning of OSN axonal projections[58–61]. However, the role of these axon guidance molecules during large-scale regeneration is not clear. For example, during development, OSNs projecting to the dorsal OB are generated early, and Sema3F secretion by these axons is repulsive to axons of later-arriving Nrp2-expressing OSN axons that therefore project to the ventral OB[61,62]. However, in this study, we saw good reinnervation of the ventral but not the dorsal OB, suggesting that different axon guidance mechanisms may be invoked following large-scale OSN ablation in adults. Elucidating the mechanisms that mediate successful vs. unsuccessful reinnervation of OSN axons may have clinical ramifications for the treatment of anosmia, as well as broader implications for therapeutic strategies to promote axon regeneration elsewhere in the nervous system.

Figures

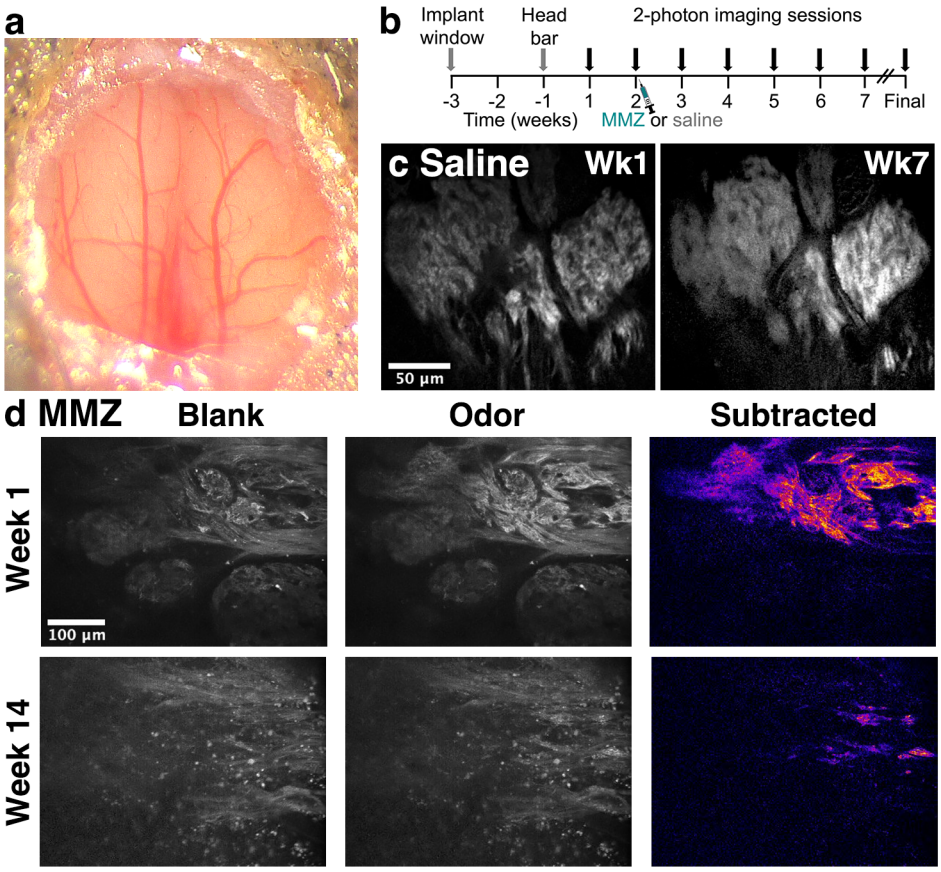

Figure 1. Chronic imaging of odorant-evoked responses in OMP-GCaMP6s mice. **a.** 3 mm diameter chronic cranial window over both OBs. **b.** Timeline for chronic imaging of OMP-GCaMP6s mice. **c.** 2-photon images showing stability of odorant-evoked responses across time in saline-injected control mice. Images are blank-subtracted responses to 1% ethyl butyrate. **d.** 2-photon images showing poor recovery of odorant-evoked responses 12 weeks after MMZ treatment. Responses to blank and odor (1% ethyl butyrate) are shown, with the blank-subtracted odor-evoked responses shown on a fire lookup table to highlight the weak responses post-MMZ.

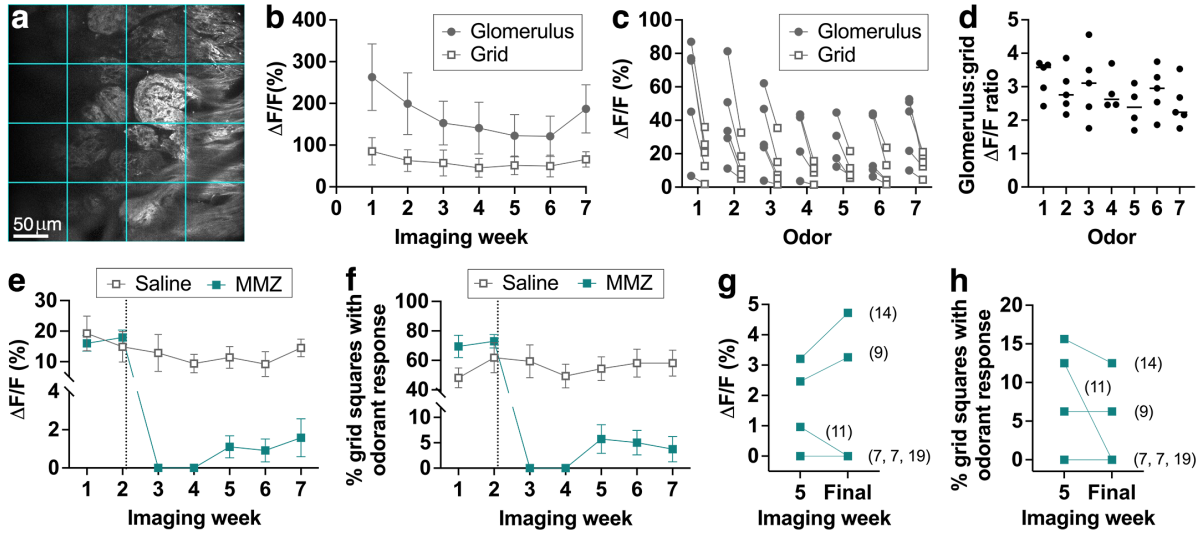

Figure 2. Poor recovery of odorant-evoked responses in dorsal OB glomeruli 10-20 weeks after MMZ treatment. a. Schematic of grid-based analysis approach. **b.** Stability of ethyl butyrate-evoked response amplitude in saline-treated OMP-GCaMP6s mice across 7 weeks of chronic imaging using glomerulus-based or grid-based analysis. Data are shown as mean ± s.e.m., n = 5 mice. **c.** Odorant-evoked response amplitude is consistently smaller across odorants for the grid-based approach. Lines connect data points for individual mice. P = 0.094, $F_{2,16}$ = 2.73 for effect of odorant; P = 0.014, $F_{1,8}$ = 9.67 for glomerulus vs. grid-based analysis; P = 0.57, $F_{6,44}$ = 0.81 for interaction; two-way ANOVA. n = 4-5 mice per odorant. Note that data is not shown for mouse-odorant pairs in which no response was detected using either approach. **d.** Ratio of odorant-evoked response amplitude for the glomerulus-based vs. grid-based approaches is similar across odorants. P = 0.55, $F_{6,26}$ = 0.84, one-way ANOVA. n as in c. **e.** Effect of MMZ on mean response amplitude across all tested odorants. Dotted line indicates injection of saline or MMZ after the second imaging session. n = 5 saline- and 6 MMZ-treated mice. **f.** Effect of MMZ on percentage of grid squares that responds to any of the tested odorants. Dotted line and n as in e. **g,h.** No further recovery of odorant-evoked responses between imaging week 5 and the final time point that could be imaged in each mouse. Numbers in parentheses indicate number of weeks for which imaging was performed. n = 6 MMZ-treated mice. **g.** Mean response amplitude across all odorants. **h.** Percentage of grid squares that responds to any of the tested odorants.

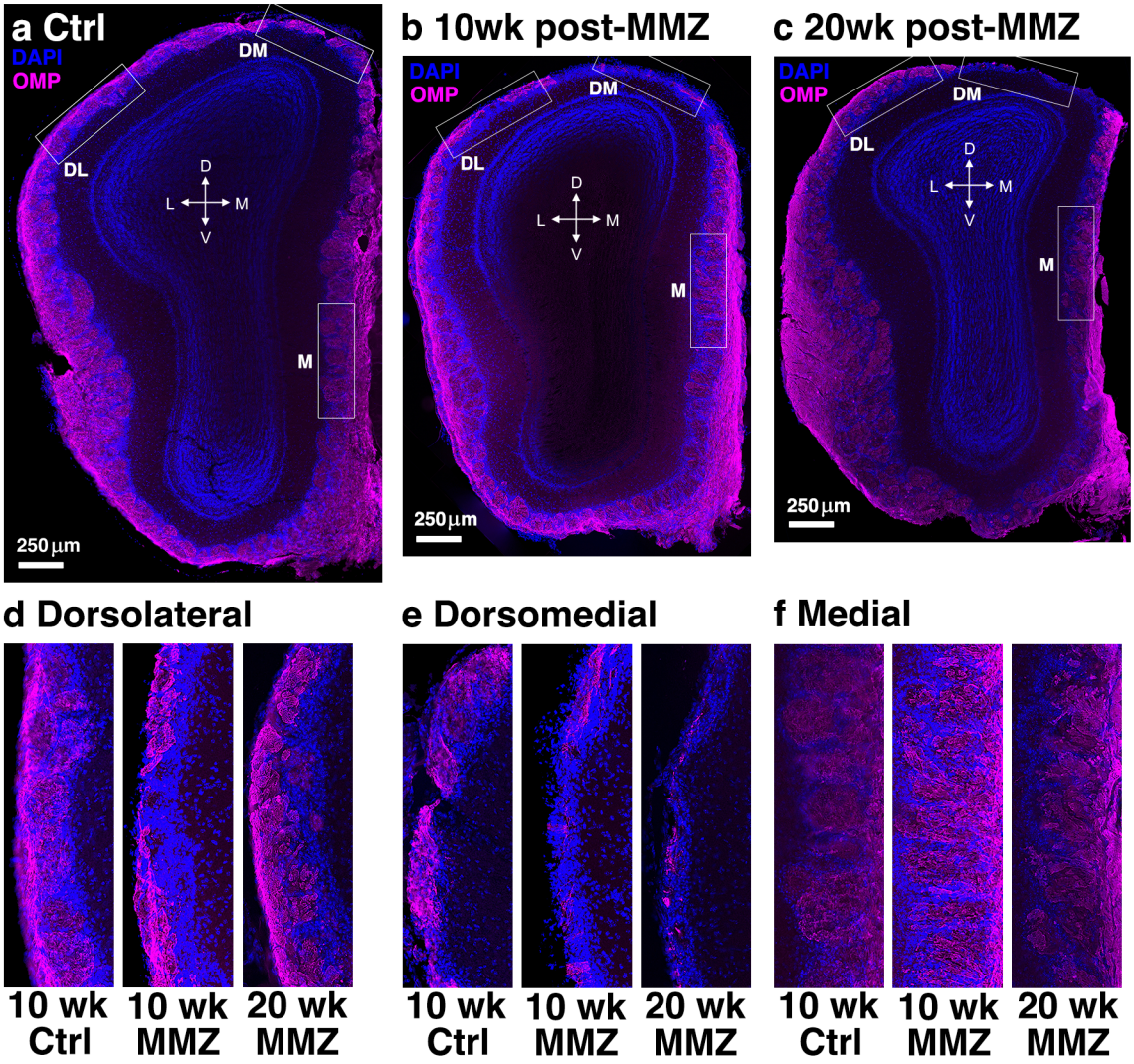

Figure 3. OMP staining reveals region-specific deficits in OSN reinnervation of the OB up to 20 weeks post-MMZ. Example widefield images of coronal OB sections stained for OMP and DAPI. **a.** Control mouse age-matched to the 10-week MMZ time point. **b.** 10-week post-MMZ mouse. **c.** 20-week post-MMZ mouse. **d.** Enlarged view of dorsolateral regions shown by boxes in a-c. **e.** Enlarged view of dorsomedial regions shown by boxes in a-c. **f.** Enlarged view of medial regions shown by boxes in a-c.

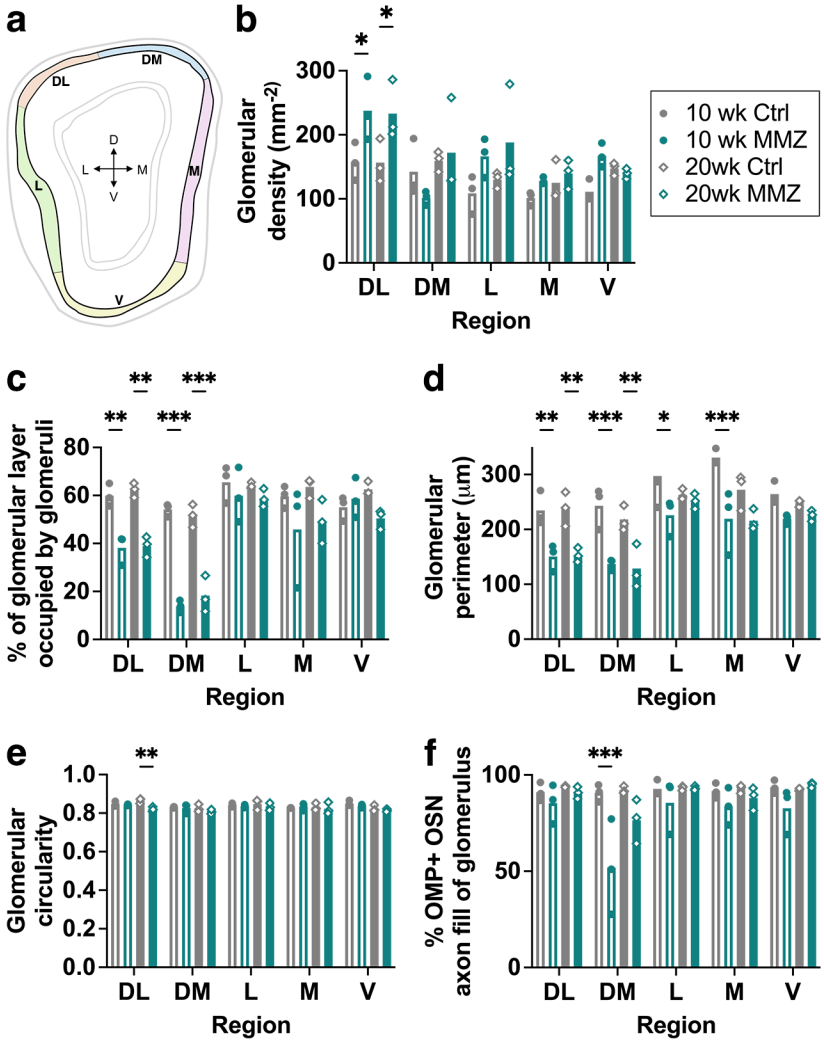

Figure 4. Region-specific deficits in regeneration of OSN axons 10-20 weeks after MMZ treatment. a. Schematic showing GL regions that were analyzed. Arrows show dorsal (D), ventral (V), medial (M) and lateral (L) directions. Analyzed regions are dorsolateral (orange), dorsomedial (blue), lateral (green), medial (pink), and ventral (yellow). **b.** Glomerular density is lower in the DL region of the GL 10 and 20 weeks post-MMZ. $P < 0.001$, $F_{4,40} = 7.04$ for GL region; $P = 0.003$, $F_{3,40}$ for effect of MMZ; $P = 0.13$, $F_{12,40} = 1.61$ for interaction, 2-way ANOVA with Holm-Sidak multiple comparisons. For 10-week control vs. MMZ: DL $P = 0.047$, $t = 2.76$; DM $P = 0.52$, $t = 1.40$; lateral $P = 0.24$, $t = 1.99$; medial $P = 0.90$, $t = 0.92$; ventral $P = 0.31$, $t = 1.94$. For 20-week control vs. MMZ: DL $P = 0.047$, $t = 2.63$; DM $P = 0.81$, $t = 0.44$; lateral $P = 0.24$, $t = 2.00$; medial $P = 0.94$, $t = 0.51$; ventral $P = 0.80$, $t = 0.28$. **c.** Percentage of the GL occupied by glomeruli is reduced in the DM and DL regions 10 and 20 weeks post-MMZ. $P < 0.001$, $F_{4,40} = 24.6$ for GL region; $P < 0.001$, $F_{3,40} = 25.9$ for effect of MMZ; $P < 0.001$, $F_{12,40} = 3.75$ for interaction, 2-way ANOVA with Holm-Sidak multiple

comparisons. For 10-week control vs. MMZ: DL P = 0.003, t = 3.62; DM P < 0.001, t = 6.74; lateral P = 0.89, t = 0.93; medial P = 0.10, t = 2.30; ventral P = 0.83, t = 0.60. For 20-week control vs. MMZ: DL P = 0.002, t = 3.90; DM P < 0.001, t = 5.55; lateral P = 0.89, t = 0.88; medial P = 0.097, t = 2.42; ventral P = 0.26, t = 2.02. **d.** Region-specific reduction in glomerular perimeter after MMZ treatment. P < 0.001, $F_{4,40}$ = 18.5 for GL region; P < 0.001, $F_{3,40}$ = 28.5 for effect of MMZ; P = 0.25, $F_{12,40}$ = 1.31 for interaction, 2-way ANOVA with Holm-Sidak multiple comparisons. For 10-week control vs. MMZ: DL P = 0.006, t = 3.48; DM P < 0.001, t = 4.38; lateral P = 0.031, t = 2.95; medial P < 0.001, t = 4.60; ventral P = 0.35, t = 1.87. For 20-week control vs. MMZ: DL P = 0.006, t = 3.50; DM P = 0.003, t = 3.68; lateral P = 0.64, t = 0.47; medial P = 0.076, t = 2.31; ventral P = 0.73, t = 0.94. **e.** Glomerular circularity is similar in MMZ-treated and control mice except for a small decrease in the DL region at 20 weeks post-MMZ. P = 0.013, $F_{4,40}$ = 3.60 for GL region; P = 0.004, $F_{3,40}$ = 5.32 for effect of MMZ; P = 0.51, $F_{12,40}$ = 0.95 for interaction, 2-way ANOVA with Holm-Sidak multiple comparisons. For 10-week control vs. MMZ: DL P = 0.8, t = 0.28; DM P = 0.96, t = 0.39; lateral P = 0.96, t = 0.46; medial P = 0.97, t = 0.62; ventral P = 0.62, t = 0.87. For 20-week control vs. MMZ: DL P = 0.008, t = 3.47; DM P = 0.56, t = 1.39; lateral P = 0.83, t = 1.16; medial P = 0.97, t = 0.67; ventral P = 0.62, t = 0.75. **f.** Selective deficit in innervation of DM glomeruli by OMP+ OSN axons. P = 0.001, $F_{4,40}$ = 5.41 for GL region; P < 0.001, $F_{3,40}$ = 9.96 for effect of MMZ; P = 0.060, $F_{12,40}$ = 1.92 for interaction. 2-way ANOVA with Holm-Sidak multiple comparisons. For 10-week control vs. MMZ: DL P = 0.93, t = 0.82; DM P < 0.001, t = 5.61; lateral P = 0.86, t = 1.04; medial P = 0.77, t = 1.15; ventral P = 0.48, t = 1.58. For 20-week control vs. MMZ: DL P = 0.96, t = 0.45; DM P = 0.084, t = 2.27; lateral P = 0.99, t = 0.01; medial P = 0.94, t = 0.68; ventral P = 0.98, t = 0.35.

Acknowledgments

This study was funded by the National Institutes on Communication Disorders and Stroke (National Institutes of Health) R01DC018516 to C.E.J.C. and F32DC018431 to T.K. We thank members of the Cheetham lab for helpful discussions.

References

1. Graziadei, P., and Graziadei, G.M. (1978). Continuous nerve cell renewal in the olfactory system. Springer-Verlag.

2. Hahn, C., Han, L., Rawson, N.E., Mirza, N., Borgmann-Winter, K., Lenox, R.H., and Arnold, S.E. (2005). In vivo and in vitro neurogenesis in human olfactory epithelium. J Comp Neurol *483*, 154–163. https://doi.org/10.1002/cne.20424.

3. Kondo, K., Suzukawa, K., Sakamoto, T., Watanabe, K., Kanaya, K., Ushio, M., Yamaguchi, T., Nibu, K., Kaga, K., and Yamasoba, T. (2010). Age-related changes in cell dynamics of the postnatal mouse olfactory neuroepithelium: Cell proliferation, neuronal differentiation, and cell death. J Comp Neurol *518*, 1962–1975. https://doi.org/10.1002/cne.22316.

4. Firestein, S. (2001). How the olfactory system makes sense of scents. Nature *413*, 211–218. https://doi.org/10.1038/35093026.

5. Buck, L., and Axel, R. (1991). A novel multigene family may encode odorant receptors: A molecular basis for odor recognition. Cell *65*, 175–187. https://doi.org/10.1016/0092-8674(91)90418-x.

6. Hanchate, N.K., Kondoh, K., Lu, Z., Kuang, D., Ye, X., Qiu, X., Pachter, L., Trapnell, C., and Buck, L.B. (2015). Single-cell transcriptomics reveals receptor transformations during olfactory neurogenesis. Science *350*, 1251–1255. https://doi.org/10.1126/science.aad2456.

7. Tan, L., Li, Q., and Xie, S.X. (2015). Olfactory sensory neurons transiently express multiple olfactory receptors during development. Molecular Systems Biology *11*, 844. https://doi.org/10.15252/msb.20156639.

8. Zamparo, I., Francia, S., Franchi, S.A., Redolfi, N., Costanzi, E., Kerstens, A., Fukutani, Y., Battistutta, R., Laureto, P.P. de, Munck, S., et al. (2019). Axonal Odorant Receptors Mediate Axon Targeting. Cell Reports *29*, 4334-4348.e7. https://doi.org/10.1016/j.celrep.2019.11.099.

9. Feinstein, P., Bozza, T., Rodriguez, I., Vassalli, A., and Mombaerts, P. (2003). Axon guidance of mouse olfactory sensory neurons by odorant receptors and the beta2 adrenergic receptor. Cell *117*, 833–846. https://doi.org/10.1016/j.cell.2004.05.013.

10. Vassar, R., Chao, S.K., Sitcheran, R., Nunez, J.M., Vosshall, L.B., and Axel, R. (1994). Topographic organization of sensory projections to the olfactory bulb. Cell *79*.

11. Ressler, K., Sullivan, S., and Buck, L. (1994). Information coding in the olfactory system: evidence for a stereotyped and highly organized epitope map in the olfactory bulb. Cell *79*, 1245–1255. https://doi.org/10.1016/0092-8674(94)90015-9.

12. Huard, J.M.T., and Schwob, J.E. (1995). Cell cycle of globose basal cells in rat olfactory epithelium. Dev. Dyn. *203*, 17–26. https://doi.org/10.1002/aja.1002030103.

13. Holl, A.-M. (2018). Survival of mature mouse olfactory sensory neurons labeled genetically perinatally. Mol Cell Neurosci *88*, 258–269. https://doi.org/10.1016/j.mcn.2018.02.005.

14. Mackay-Sim, A., and Kittel, P. (1991). On the Life Span of Olfactory Receptor Neurons. Eur J Neurosci *3*, 209–215.

15. Hinds, J.W., Hinds, P.L., and McNelly, N.A. (1984). An autoradiographic study of the mouse olfactory epithelium: Evidence for long-lived receptors. The Anatomical Record *210*, 375–383. https://doi.org/10.1002/ar.1092100213.

16. Leung, C.T., Coulombe, P.A., and Reed, R.R. (2007). Contribution of olfactory neural stem cells to tissue maintenance and regeneration. Nature Neuroscience *10*, 720–726. https://doi.org/10.1038/nn1882.

17. Iwai, N., Zhou, Z., Roop, D.R., and Behringer, R.R. (2008). Horizontal Basal Cells Are Multipotent Progenitors in Normal and Injured Adult Olfactory Epithelium. STEM CELLS *26*, 1298–1306. https://doi.org/10.1634/stemcells.2007-0891.

18. Gadye, L., Das, D., Sanchez, M.A., Street, K., Baudhuin, A., Wagner, A., Cole, M.B., Choi, Y., Yosef, N., Purdom, E., et al. (2017). Injury Activates Transient Olfactory Stem Cell States with Diverse Lineage Capacities. Cell Stem Cell *21*, 775-790.e9. https://doi.org/10.1016/j.stem.2017.10.014.

19. Savya, S.P., Kunkhyen, T., and Cheetham, C. (2019). Low survival rate of young adult-born olfactory sensory neurons in the undamaged mouse olfactory epithelium. J. Bioenerg. Biomembr. *51*, 41–51. https://doi.org/10.1007/s10863-018-9774-8.

20. Liberia, T., Martin-Lopez, E., Meller, S.J., and Greer, C.A. (2019). Sequential maturation of olfactory sensory neurons in the mature olfactory epithelium. Eneuro *6*, ENEURO.0266-19.2019. https://doi.org/10.1523/eneuro.0266-19.2019.

21. Rodriguez-Gil, D.J., Bartel, D.L., Jaspers, A.W., Mobley, A.S., Imamura, F., and Greer, C.A. (2015). Odorant receptors regulate the final glomerular coalescence of olfactory sensory neuron axons. Proc Natl Acad Sci *112*, 5821–5826. https://doi.org/10.1073/pnas.1417955112.

22. Miragall, F., and Graziadei, G.M. (1982). Experimental studies on the olfactory marker protein. II. Appearance of the olfactory marker protein during differentiation of the olfactory sensory neurons of mouse: an immunohistochemical and autoradiographic study. Brain Res *239*, 245–250. https://doi.org/10.1016/0006-8993(82)90846-0.

23. Doucette, J.R., Kiernan, J.A., and Flumerfelt, B.A. (1983). The re-innervation of olfactory glomeruli following transection of primary olfactory axons in the central or peripheral nervous system. J. Anat. *137 (Pt 1)*, 1–19.

24. Graziadei, P.P.C., and Graziadei, G.A.M. (1979). Neurogenesis and neuron regeneration in the olfactory system of mammals. I. Morphological aspects of differentiation and structural organization of the olfactory sensory neurons. J. Neurocytol. *8*, 1–18. https://doi.org/10.1007/bf01206454.

25. Cummings, D.M., Emge, D.K., Small, S.L., and Margolis, F.L. (2000). Pattern of olfactory bulb innervation returns after recovery from reversible peripheral deafferentation. J. Comp. Neurol. *421*, 362–373. https://doi.org/10.1002/(sici)1096-9861(20000605)421:3<362::aid-cne5>3.0.co;2-8.

26. Schwob, J.E., Youngentob, S.L., Ring, G., Iwema, C.L., and Mezza, R.C. (1999). Reinnervation of the rat olfactory bulb after methyl bromide-induced lesion: Timing and extent of reinnervation. Journal of Comparative Neurology *412*, 439–457. https://doi.org/10.1002/(sici)1096-9861(19990927)412:3<439::aid-cne5>3.0.co;2-h.

27. Burd, G.D. (1993). Morphological study of the effects of intranasal zinc sulfate Irrigation on the Mouse Olfactory Epithelium and Olfactory Bulb. *24*, 195–213.

28. Bergman, U., Östergren, A., Gustafson, A.-L., and Brittebo, E. (2002). Differential effects of olfactory toxicants on olfactory regeneration. Archives of Toxicology *76*, 104–112. https://doi.org/10.1007/s00204-002-0321-2.

29. Browne, L.P., Crespo, A., and Grubb, M.S. (2022). Rapid presynaptic maturation in naturally regenerating axons of the adult mouse olfactory nerve. Cell Rep. *41*, 111750. https://doi.org/10.1016/j.celrep.2022.111750.

30. Kikuta, S., Sakamoto, T., Nagayama, S., Kanaya, K., Kinoshita, M., Kondo, K., Tsunoda, K., Mori, K., and Yamasoba, T. (2015). Sensory Deprivation Disrupts Homeostatic Regeneration of Newly Generated Olfactory Sensory Neurons after Injury in Adult Mice. J. Neurosci. *35*, 2657–2673. https://doi.org/10.1523/jneurosci.2484-14.2015.

31. Nakamura, Y., Miwa, T., Shiga, H., Sakata, H., Shigeta, D., and Hatta, T. (2024). Histological changes in the olfactory bulb and rostral migratory stream due to interruption of olfactory input. Auris Nasus Larynx *51*, 517–524. https://doi.org/10.1016/j.anl.2024.01.009.

32. Kunkhyen, T., Brechbill, T.R., Berg, S.P.R., Pothuri, P., Rangel, A.N., Gupta, A., and Cheetham, C.E.J. (2024). Cell type- and layer-specific plasticity of olfactory bulb interneurons following olfactory sensory neuron ablation. Sci. Rep. *14*, 17771. https://doi.org/10.1038/s41598-024-68649-4.

33. Gogos, J.A., Osborne, J., Nemes, A., Mendelsohn, M., and Axel, R. (2000). Genetic Ablation and Restoration of the Olfactory Topographic Map. Cell *103*, 609–620. https://doi.org/10.1016/s0092-8674(00)00164-1.

34. Costanzo, R., and Graziadei, P. (1983). A quantitative analysis of changes in the olfactory epithelium following bulbectomy in hamster. The Journal of comparative neurology *215*, 370–381. https://doi.org/10.1002/cne.902150403.

35. John, J.A.S., and Key, B. (2003). Axon Mis-targeting in the Olfactory Bulb During Regeneration of Olfactory Neuroepithelium. Chem. Senses *28*, 773–779. https://doi.org/10.1093/chemse/bjg068.

36. Carr, V.M., Ring, G., Youngentob, S.L., Schwob, J.E., and Farbman, A.I. (2004). Altered epithelial density and expansion of bulbar projections of a discrete HSP70 immunoreactive subpopulation of rat olfactory receptor neurons in reconstituting olfactory epithelium following exposure to methyl bromide. Journal of Comparative Neurology *469*. https://doi.org/10.1002/cne.11020.

37. Blanco-Hernández, E., Valle-Leija, P., Zomosa-Signoret, V., Drucker-Colín, R., and Vidaltamayo, R. (2012). Odor memory stability after reinnervation of the olfactory bulb. PloS One *7*, e46338. https://doi.org/10.1371/journal.pone.0046338.

38. Cheung, M.C., Jang, W., Schwob, J.E., and Wachowiak, M. (2014). Functional recovery of odor representations in regenerated sensory inputs to the olfactory bulb. Frontiers in Neural Circuits *7*, 207. https://doi.org/10.3389/fncir.2013.00207.

39. Yu, C., Power, J., Barnea, G., O'Donnell, S., and Neuron, H. (2004). Spontaneous neural activity is required for the establishment and maintenance of the olfactory sensory map.

40. Wekselblatt, J.B., Flister, E.D., Piscopo, D.M., and Niell, C.M. (2016). Large-scale imaging of cortical dynamics during sensory perception and behavior. J Neurophysiol *115*, 2852–2866. https://doi.org/10.1152/jn.01056.2015.

41. Madisen, L., Zwingman, T.A., Sunkin, S.M., Oh, S.W., Zariwala, H.A., Gu, H., Ng, L.L., Palmiter, R.D., Hawrylycz, M.J., Jones, A.R., et al. (2009). A robust and high-throughput Cre reporting and characterization system for the whole mouse brain. Nat Neurosci *13*, 133–140. https://doi.org/10.1038/nn.2467.

42. Daigle, T.L., Madisen, L., Hage, T.A., Valley, M.T., Knoblich, U., Larsen, R.S., Takeno, M.M., Huang, L., Gu, H., Larsen, R., et al. (2018). A Suite of Transgenic Driver and Reporter Mouse Lines with Enhanced Brain-Cell-Type Targeting and Functionality. Cell *174*, 465-480.e22. https://doi.org/10.1016/j.cell.2018.06.035.

43. Haddad, R., Lanjuin, A., Madisen, L., Zeng, H., Murthy, V.N., and Uchida, N. (2013). Olfactory cortical neurons read out a relative time code in the olfactory bulb. Nat. Neurosci. *16*, 949–957. https://doi.org/10.1038/nn.3407.

44. Cheetham, C.E., Park, U., and Belluscio, L. (2016). Rapid and continuous activity-dependent plasticity of olfactory sensory input. Nature communications *7*, 10729. https://doi.org/10.1038/ncomms10729.

45. Cheetham, C.E. (2018). Multiphoton intravital calcium imaging. Curr. Protoc. Cytom. *e40*, doi: 10.1002/cpcy.40.

46. Schindelin, J., Arganda-Carreras, I., Frise, E., Kaynig, V., Longair, M., Pietzsch, T., Preibisch, S., Rueden, C., Saalfeld, S., Schmid, B., et al. (2012). Fiji: an open-

source platform for biological-image analysis. Nature Methods *9*, 676–682. https://doi.org/10.1038/nmeth.2019.

47. Huang, J.S., Kunkhyen, T., Rangel, A.N., Brechbill, T.R., Gregory, J.D., Winson-Bushby, E.D., Liu, B., Avon, J.T., Muggleton, R.J., and Cheetham, C.E.J. (2022). Immature olfactory sensory neurons provide behaviourally relevant sensory input to the olfactory bulb. Nat. Commun. *13*, 6194. https://doi.org/10.1038/s41467-022-33967-6.

48. Ross, J.M., and Fletcher, M.L. (2018). Learning-Dependent and -Independent Enhancement of Mitral/Tufted Cell Glomerular Odor Responses Following Olfactory Fear Conditioning in Awake Mice. Journal of Neuroscience *38*. https://doi.org/10.1523/jneurosci.3559-17.2018.

49. Kass, M.D., Rosenthal, M.C., Pottackal, J., and McGann, J.P. (2013). Fear learning enhances neural responses to threat-predictive sensory stimuli. Science (New York, N.Y.) *342*. https://doi.org/10.1126/science.1244916.

50. Czarnecki, L.A., Moberly, A.H., Turkel, D.J., Rubinstein, T., Pottackal, J., Rosenthal, M.C., McCandlish, E.F.K., Buckley, B., and McGann, J.P. (2012). Functional Rehabilitation of Cadmium-Induced Neurotoxicity Despite Persistent Peripheral Pathophysiology in the Olfactory System. Toxicol. Sci. *126*, 534–544. https://doi.org/10.1093/toxsci/kfs030.

51. Jang, W., Youngentob, S.L., and Schwob, J.E. (2003). Globose basal cells are required for reconstitution of olfactory epithelium after methyl bromide lesion. J. Comp. Neurol. *460*, 123–140. https://doi.org/10.1002/cne.10642.

52. Kobayakawa, K., Kobayakawa, R., Matsumoto, H., Oka, Y., Imai, T., Ikawa, M., Okabe, M., Ikeda, T., Itohara, S., Kikusui, T., et al. (2007). Innate versus learned odour processing in the mouse olfactory bulb. Nature *450*, 503–508. https://doi.org/10.1038/nature06281.

53. Matsumoto, H., Kobayakawa, K., Kobayakawa, R., Tashiro, T., Mori, K., Sakano, H., and Mori, K. (2010). Spatial Arrangement of Glomerular Molecular-Feature Clusters in the Odorant-Receptor Class Domains of the Mouse Olfactory Bulb. J. Neurophysiol. *103*, 3490–3500. https://doi.org/10.1152/jn.00035.2010.

54. Tsai, L., and Barnea, G. (2014). A Critical Period Defined by Axon-Targeting Mechanisms in the Murine Olfactory Bulb. Science *344*, 197–200. https://doi.org/10.1126/science.1248806.

55. Ma, L., Wu, Y., Qiu, Q., Scheerer, H., Moran, A., and Yu, C.R. (2014). A Developmental Switch of Axon Targeting in the Continuously Regenerating Mouse Olfactory System. Science *344*, 194–197. https://doi.org/10.1126/science.1248805.

56. Wu, Y., Ma, L., Duyck, K., Long, C.C., Moran, A., Scheerer, H., Blanck, J., Peak, A., Box, A., Perera, A., et al. (2018). A Population of Navigator Neurons Is Essential for Olfactory Map Formation during the Critical Period. Neuron *100*, 1066-1082.e6. https://doi.org/10.1016/j.neuron.2018.09.051.

57. Carr, V.M., Ring, G., Youngentob, S.L., Schwob, J.E., and Farbman, A.I. (2004). Altered epithelial density and expansion of bulbar projections of a discrete HSP70 immunoreactive subpopulation of rat olfactory receptor neurons in reconstituting olfactory epithelium following exposure to methyl bromide. J. Comp. Neurol. *469*, 475–493. https://doi.org/10.1002/cne.11020.

58. Nguyen-Ba-Charvet, K.T., Meglio, T.D., Fouquet, C., and Chédotal, A. (2008). Robos and Slits Control the Pathfinding and Targeting of Mouse Olfactory Sensory Axons. J. Neurosci. *28*, 4244–4249. https://doi.org/10.1523/jneurosci.5671-07.2008.

59. Norlin, E.M., Alenius, M., Gussing, F., Hägglund, M., Vedin, V., and Bohm, S. (2001). Evidence for Gradients of Gene Expression Correlating with Zonal Topography of the Olfactory Sensory Map. Mol. Cell. Neurosci. *18*, 283–295. https://doi.org/10.1006/mcne.2001.1019.

60. Cho, J.H., Lépine, M., Andrews, W., Parnavelas, J., and Cloutier, J.-F. (2007). Requirement for Slit-1 and Robo-2 in Zonal Segregation of Olfactory Sensory Neuron Axons in the Main Olfactory Bulb. J. Neurosci. *27*, 9094–9104. https://doi.org/10.1523/jneurosci.2217-07.2007.

61. Takeuchi, H., Inokuchi, K., Aoki, M., Suto, F., Tsuboi, A., Matsuda, I., Suzuki, M., Aiba, A., Serizawa, S., Yoshihara, Y., et al. (2010). Sequential arrival and graded secretion of Sema3F by olfactory neuron axons specify map topography at the bulb. Cell *141*, 1056–1067. https://doi.org/10.1016/j.cell.2010.04.041.

62. Eerdunfu, Ihara, N., Ligao, B., Ikegaya, Y., and Takeuchi, H. (2017). Differential timing of neurogenesis underlies dorsal-ventral topographic projection of olfactory sensory neurons. Neural Dev *12*, 2. https://doi.org/10.1186/s13064-017-0079-0.